Title

Mutation of a kinase allosteric node uncouples dynamics linked to phosphotransfer

Journal

Proceedings of the National Academy of Sciences of the United States of America, 114(6)

ISSN

0027-8424

Authors

Ahuja, Lalima G
Kornev, Alexandr P
McClendon, Christopher L
et al.

Publication Date

2017-02-07

DOI

10.1073/pnas.1620667114

Peer reviewed

Mutation of a kinase allosteric node uncouples dynamics linked to phosphotransfer

Lalima G. Ahuja[a], Alexandr P. Kornev[a], Christopher L. McClendon[b], Gianluigi Veglia[c,d], and Susan S. Taylor[a,e,1]

[a]Department of Pharmacology, University of California, San Diego, La Jolla, CA 92093; [b]Cardiovascular and Metabolic Diseases, Medicinal Chemistry, Pfizer Biomedical Institute, Pfizer, Inc., Cambridge, MA 02139; [c]Department of Chemistry, University of Minnesota, Minneapolis, MN 55455; [d]Department of Biochemistry, Molecular Biology, and Biophysics, University of Minnesota, Minneapolis, MN 55455; and [e]Department of Chemistry and Biochemistry, University of California, San Diego, La Jolla, CA 92093

Contributed by Susan S. Taylor, December 20, 2016 (sent for review November 22, 2016; reviewed by Amy Andreotti and Ruth Nussinov)

The expertise of protein kinases lies in their dynamic structure, wherein they are able to modulate cellular signaling by their phosphotransferase activity. Only a few hundreds of protein kinases regulate key processes in human cells, and protein kinases play a pivotal role in health and disease. The present study dwells on understanding the working of the protein kinase-molecular switch as an allosteric network of "communities" composed of congruently dynamic residues that make up the protein kinase core. Girvan–Newman algorithm-based community maps of the kinase domain of cAMP-dependent protein kinase A allow for a molecular explanation for the role of protein conformational entropy in its catalytic cycle. The community map of a mutant, Y204A, is analyzed vis-à-vis the wild-type protein to study the perturbations in its dynamic profile such that it interferes with transfer of the γ-phosphate to a protein substrate. Conventional biochemical measurements are used to ascertain the effect of these dynamic perturbations on the kinetic profiles of both proteins. These studies pave the way for understanding how mutations far from the kinase active site can alter its dynamic properties and catalytic function even when major structural perturbations are not obvious from static crystal structures.

allostery | community maps | protein kinases | catalytic cycle | protein dynamics

Eukaryotic protein kinases (EPKs) constitute ∼2% of the human genome and regulate key cell functions including growth, metabolism, DNA repair, signaling, and cell division (1). These highly specialized and regulated enzymes work by transferring the γ-phosphate of ATP to a designated Ser/Thr/Tyr in a substrate protein (2, 3). Although evolved in their substrate specificity, EPKs are not optimized for catalytic efficiency. They work as molecular switches that control the modifications of their target proteins (3). The structural framework of their switching mechanism has been detailed for various EPKs including cAMP-dependent protein kinase A (PKA) (2). In addition, EPKs are themselves regulated by chemical modifications, conformational change, and also ligand binding to respond to changes in environment and input signals (2).

The structural core of the EPKs harbors a conserved active site formed between the cleft of a bilobal structure (4). The small lobe is predominantly made up of a β-sheet and a conserved αC-helix, whereas the large lobe is made up mostly of α-helices that anchor two small β-sheets at the active-site cleft (2). Two hydrophobic "spines," anchored to the hydrophobic αF-helix, form a structural motif that connects the two lobes of the kinase core (Fig. 1). The assembled regulatory "R spine" is the hallmark signature of an active kinase, and the disassembled–assembled R-spine switch constitutes the dynamic link between kinase inactivation–activation (5). The catalytic "C spine" is completed by binding of the ATP adenine ring that primes the kinase for catalysis (5, 6). Phosphorylation of an activation loop in the large lobe forms an almost universal mechanism for EPK regulation (7, 8). This phosphate moiety couples both lobes of the kinase core and facilitates the assembly of the R spine, thus stabilizing the active conformation (8), which can now toggle between the open and closed states that are associated with catalysis. Synergistic cross talk is required between the ATP-binding site and the peptide-binding site for a concerted phosphorylation event. ATP binding that completes the C spine is accompanied by compactness of the kinase domain by associated spatial rearrangement of residues lining the ATP-binding pocket (9). Engagement of the glycine-rich loop, β3-stand, the αC-helix allows for a twisting of the small lobe that leads to the closure of the active-site cleft in response to ATP binding. This brings the γ-phosphate in close proximity to the catalytic residues and engages the αC-helix with the activation loop phosphorylation site.

In recent years, important progress has been made in studying the open, intermediate, and closed states of EPKs (especially PKA) (10–13). Structural characterizations also include many inhibitor-bound kinases for pharmaceutical drug discovery. However, just like other proteins, these EPK structures actually fluctuate in energy landscapes whose minima typically correspond to these X-ray snapshots. Molecular fluctuations defining these energy landscapes contribute to the "conformational entropy" of proteins that reflects their internal dynamics (14). This entropy is a global property of the protein inclusive of its side-chain motions, main-chain motions, and secondary-structure conformations. Although this global protein conformational entropy explains modulation of free energy of protein–ligand/substrate binding, it is often masked by the static crystal structures. Binding of a ligand to a protein like EPKs typically requires its transition from a higher (disordered) to a lower (structured, bound) state that uses this conformational entropy of the protein macromolecule (14). Although this simplistic theoretical decomposition of confrontational entropy may be used to explain protein–ligand binding, its experimental validation by techniques like NMR is complex and can only be understood in part. A linear relationship between conformational entropy and ligand binding entropy has been attempted by NMR for various proteins including

Significance

Our Girvan–Newman-based community network analysis provides a strategy to explore the effects of protein kinase mutations on the dynamic properties of the kinase core and the allosteric network underlying the catalytic cycle. With this approach, which allows us to identify subtle shifts in dynamics and in particular side-chain rotamer preferences, we can explain the underlying mechanism for loss of function in many different scenarios. Our method is especially relevant for disease-causing mutations that lie far from the active site but show no obvious structural perturbations based on X-ray crystallography.

Author contributions: L.G.A., A.P.K., and S.S.T. designed research; L.G.A. and C.L.M. performed research; L.G.A., A.P.K., C.L.M., and S.S.T. contributed new reagents/analytic tools; L.G.A., A.P.K., G.V., and S.S.T. analyzed data; and L.G.A., A.P.K., G.V., and S.S.T. wrote the paper.

Reviewers: A.A., Iowa State University; and R.N., National Cancer Institute.

The authors declare no conflict of interest.

[1]To whom correspondence should be addressed. Email: staylor@ucsd.edu.

This article contains supporting information online at www.pnas.org/lookup/suppl/doi:10.1073/pnas.1620667114/-/DCSupplemental.

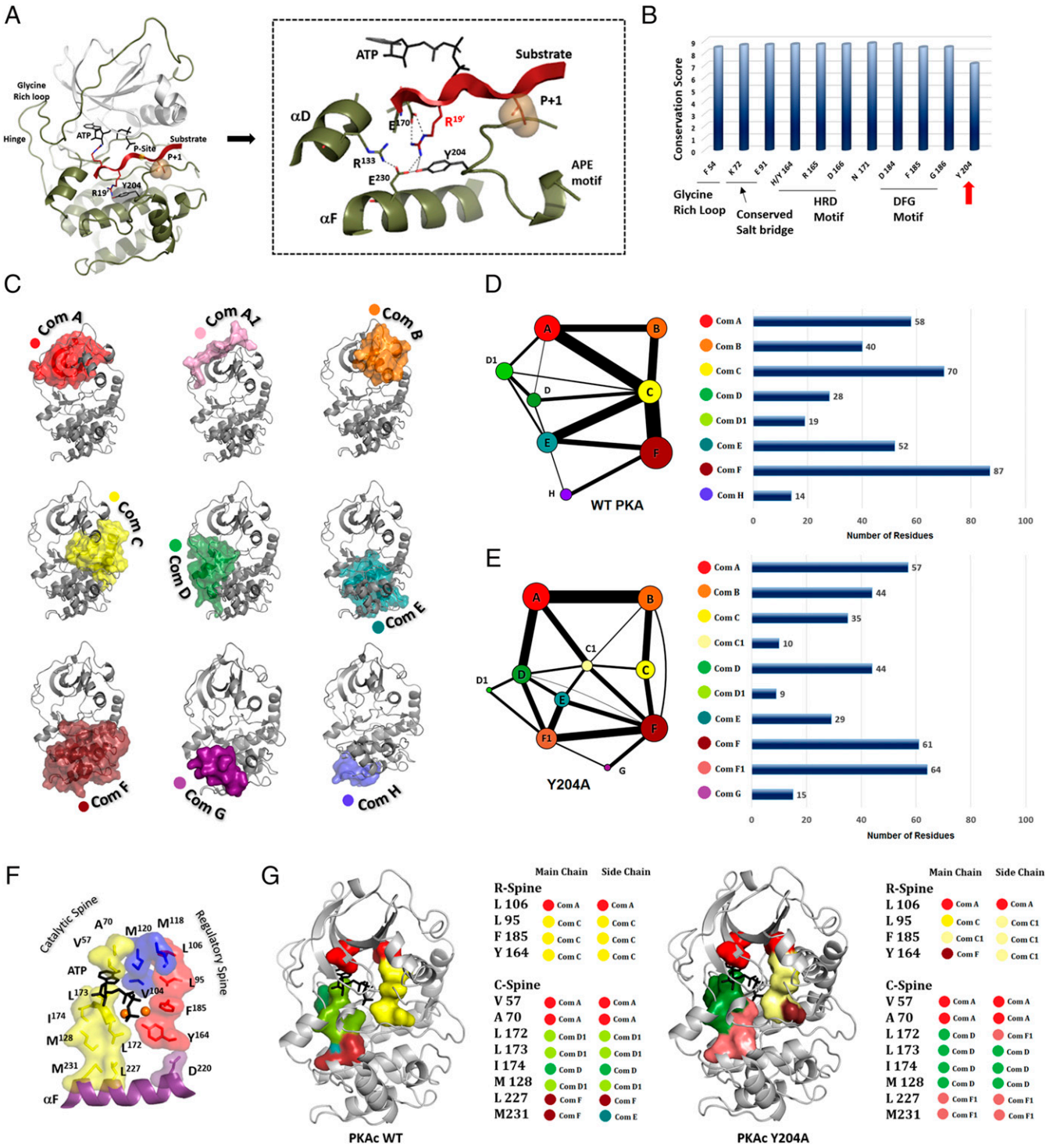

Fig. 1. The Y204A node: sequence conservation, structural role, and dynamic changes in PKA. (*A*) Position of the Y204 residue in the C lobe of PKA kinase. Y204 is adjacent to the P+1 loop and makes extensive hydrogen interactions with key residues including E230 from the αF-helix that supports the kinase spines. (*B*) Sequence conservation score for Y204 across the kinome. The residue is almost as conserved as other key elements of the kinase structure like the conserved K72-E91 salt bridge, the DFG motif, and HRD motif. In AGC kinases, this residue is usually a Tyr, whereas in some tyrosine kinases it is a Trp. (*C*) Communities detected in the allosteric network of PKA kinase mapped onto its structure. Each community is around 75 residues big but is smaller than a subdomain. Functional roles of communities are provided in detail in Fig. S1. (*D*) Communities and their residue populations detected for the wtPKA:ATP:1Mg^{2+} complex. (*E*) Communities and their residue populations detected for Y204A:ATP:1Mg^{2+} complex. (*F*) Hydrophobic spines that connect the two lobes of the kinase domain. (*G*) Community distribution of the main chains and side chains of the hydrophobic spine residues in the wtPKA and Y204A.

calmodulin (15), catabolite activator protein (16), and also PKA (17). The correlation between conformational entropy and enzyme catalysis is even more complex and challenging to study. In the case of protein kinases, the complete enzyme catalytic cycle must simultaneously and synchronously use both slow and fast dynamic aspects of the protein's conformational entropy (3). Crystallography,

NMR, and computational approaches all contribute in specific and unique ways to our understanding of this complex allosteric process.

In the present study, we explore the role of conformational entropy of PKA in its catalytic cycle by comparing the wild-type C-subunit (wtPKA) to a catalytically deficient mutant Y204A using both biochemical experiments and molecular dynamics (MD) simulations. Y204A is of particular interest, as it lies far from the active site, binds both nucleotide and substrate (18), and has a protein–ligand structure that is almost identical to wtPKA (19). This mutant has also been characterized by NMR where it shows distinct differences in spin relaxations on ligand binding compared with wtPKA (20, 21). Despite all these characterizations, the role of this mutation in disrupting PKA catalytic activity is not clearly understood. In the present study, we biochemically characterize the molecular cooperativity between nucleotide and peptide binding for wtPKA and Y204A and explain the unknown role of this mutation in altering nucleotide–substrate synergy at the kinase active site. These biochemical studies then provide a framework for analysis of conformational entropy in PKA's catalytic cycle. Conformational entropy is studied for both wtPKA and the Y204A mutant using community analysis (22) where the Girvan Newman algorithm is used to identify functional ensembles called "communities" in the protein microsecond simulations based on the mutual informational matrices obtained for the structures' internal dynamics. This community network model can reflect the conformational entropy of the molecule and has been recently gaining appreciation as a way to understand dynamics-based protein allostery in various proteins including thrombin (23), Tec kinases (24), and also PKA (22). By building on our earlier models for community-based networks for the wtPKA (22, 25), we provide a dynamic conformational entropy-based explanation for the disruption of catalytic activity in PKA by a single point mutation that lies far from the active site. We carry out this comparison for the catalytically competent ATP-bound states of both wild-type and Y204A structures. This study provides a link between enzyme catalysis and protein conformational entropy and opens up fresh avenues for understanding EPKs in general and in particular the role of distal mutations that are linked to disease.

Results

Community Map of the Conserved Eukaryotic Kinase Domain Explains the Allosteric Functioning of Protein Kinases. The conserved kinase core, first defined by the structure of PKA (26–28), is a bilobal structure that brings together two substrates (nucleotide and peptide/protein) at its active-site cleft to generate a phosphorylated product. Our mechanistic understanding of these enzymes is limited by simplification of these structures as rigid bodies that do not allow for molecular explanations of subtleties in kinase function. In an effort to understand the internal allosteric networks that weave a kinase into a functional module, we have recently used a community analysis that clusters the PKA residues into functionally distinct groups called communities (22). These community maps, coupled with crystal structures and NMR analyses, provide a more comprehensive perspective for understanding the protein kinase core as an ensemble of communities that must work coherently with each other to yield the required function. Each community is composed of up to 75 residues that are allosterically coupled to each other and also to other communities via a dynamic network. These network maps hence allow for dynamically tying-in all residues of the kinase structure, including those far away from the active site (Fig. 1 and Figs. S1 and S2).

For the present study, we focused on the Y204A mutation that was previously characterized by a crystal structure of a ternary complex that is almost identical to the wtPKA (18, 19, 29). Although Y204 located in the P+1 loop has no direct contact with the peptide substrate, crystal structures reveal the direct coupling of the P+1 loop via Y204 to E230 and to the hydrophobic core (Fig. 1 and Figs. S1 and S2). The structure, however, does not explain the loss the phosphotransfer activity (30) in the mutant as this Y204 node is 17.7 Å away from the γ-phosphate of ATP that is bound at the active site (Fig. 1). We hence undertook MD simulations of the Y204A mutant in an effort to understand the role of internal dynamics and its dependence on conformational entropy that might help us to elucidate the role of the mutation. We performed a community analysis of this mutant and compared it to that of the community network of wtPKA (Fig. 1 and Fig. S1). Interestingly, the effect of a single mutation of Y204 to Ala has a major effect on the distribution of communities in the kinase core. The Y204A community network splits the number of communities into 10 groups, as opposed to 8 groups in the wild-type structure. The splitting of ComF [community for substrate binding (Figs. S1 and S2)] into ComF and ComF1 is rationalized by the presence of Y204 in ComF. However, the extensive rearrangement of communities around ComF and ComF1 leads to a total increase in the number of residues in these groups (87 in the wtPKA vs. 125 in the Y204A). The protein–protein interaction community (ComH) is lost in the mutant to be replaced by the regulatory-subunit binding community (ComG). The signal integrating ComC centered around the αC-helix is also split up in the Y204A mutant into ComC and ComC1. The ATP binding/catalytic communities ComD and ComD1 are also extensively reorganized and more populated in the Y204A mutant compared with the tPKA. This community network analysis shows crucial reorganization of protein dynamic allostery in a conserved protein structure due to a single point mutation. What are the catalytic consequences of these perturbations?

Y204A Cleaves ATP in the Hydrolysis Reaction but Cannot Do Efficient Phosphotransfer. To understand the mechanistic implications of the Y204A mutation, we needed to do an extensive biochemical characterization of the protein and compare it to wtPKA. The phosphotransfer activity of the recombinant Y204A mutant was tested using the PKA-specific peptide, Kemptide (Fig. 2). Y204A showed a remarkably lower efficiency (~70-fold decrease in k_{cat}/K_m) in transferring the phosphate from ATP to Kemptide with a turnover of only 0.33 s^{-1}. Because the Michaelis–Menten constant (K_m) for ATP was not significantly altered (26.8 ± 2.5 μM for Y204A vs. 34.1 ± 0.2 μM for wtPKA), pre–steady-state kinetics was measured to determine the burst phase of the catalytic cycle, which is a signature catalytic feature for wtPKA (3). The burst phase represents the first single phosphotransfer in the catalytic cycle when the enzyme:bisubstrate complex has yet not attained a steady state for wtPKA. This rate is higher than the steady-state rate k_{cat} where ADP release becomes rate limiting (3). Y204A lacked this signature burst phase and has an extremely low k_{cat} (Fig. 2), indicating that its kinetics was crucially altered such that ADP release is no longer likely to be the rate-limiting step of the phosphotransfer cycle. This assay also suggests an altered protein dynamics, which may be underlying an altered catalytic cycle.

The low phosphotransfer efficiency of the Y204A mutant seen in our biochemical studies, and the trapping of ADP and phosphate in the Y204A crystal structure reported earlier (19), prompted us to also study ATP hydrolysis for this mutant. For this assay, we detected the phosphate released upon incubation of the protein with ATP in the absence of any receiver substrate peptide. Intriguingly, although Y204A was severely deficient in transferring the phosphate to the peptide substrate, it could still transfer the phosphate to a water molecule at its active site (Fig. 2). The ATPase activity of Y204A was comparable to that of the wild-type protein (k_{cat} of 62.2 ± 3.1 min^{-1} for Y204A vs. 83.7 ± 1.2 min^{-1} for wtPKA). The half-life of the ATPase reaction for the Y204A mutant was only 1.5-fold longer than for wtPKA ($T_{1/2}$ of 0.61 min for wtPKA and 0.91 min for Y204A). However, Y204A did show a 10-fold increase in the K_m for ATP in the ATPase reaction (218.1 ± 24.5 μM for Y204A vs. 26.9 ± 1.1 μM for wtPKA),

indicating an altered ATPase reaction at the active site compared with wtPKA. In any case, the reduced capacity of this mutant to transfer the γ-phosphate from ATP to a protein substrate while retaining its capacity to transfer the phosphate to water is potentially consistent with seeing the ATP hydrolysis in the Y204A crystal.

Y204A Binds Nucleotides and the Pseudosubstrate Inhibitor Peptide IP20 at Its Active Site. As Y204A showed ATPase activity comparable to the wtPKA, its binding to nucleotides ATP, ADP, and AMP-PNP was studied by measuring the intrinsic tryptophan fluorescence of the protein. Compared with the wtPKA, Y204A

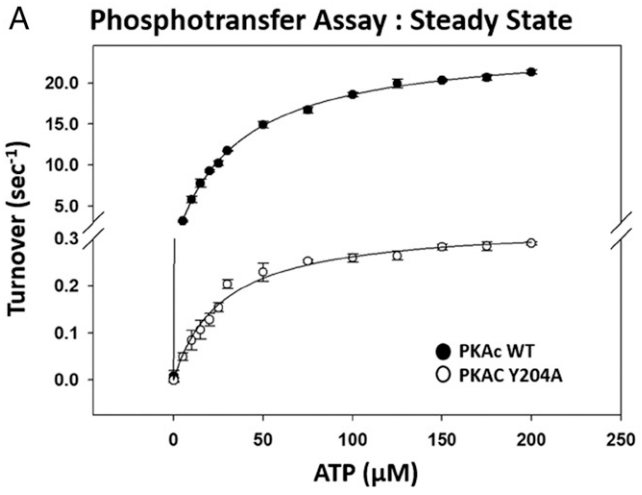

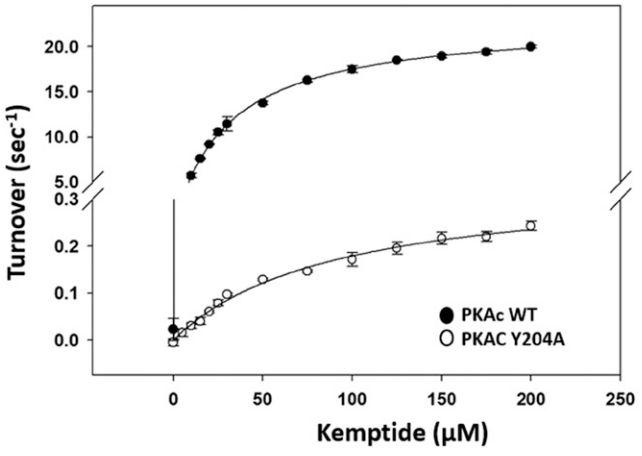

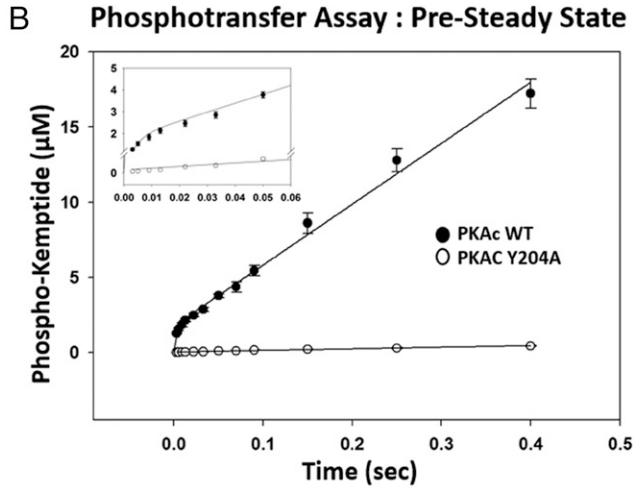

C

	PKAc WT	PKAc Y204A
Phosphotransfer		
k_{cat} (sec^{-1})	24.9 ± 0.2	0.33 ± 0.01
K_M ATP(μM)	34.1 ± 0.2	26.8 ± 2.5
K_M Kemptide(μM)	30.3 ± 0.6	90.2 ± 8.7
Burst Amplitude (sec^{-1})	285.3 ± 17.8	None
k_{cat}/K_M ($M^{-1}sec^{-1}$)	73.6 x 10^4	1.22 x 10^4
ATPase Activity		
$T_{1/2}$ (min)	0.61	0.91
k_{cat} (min^{-1}) X 10^{-2}	83.7 ± 1.2	62.2 ± 3.1
K_M ATP(μM)	26.9 ± 1.1	218.1 ± 24.5
k_{cat}/K_M ($M^{-1}sec^{-1}$) X 10^{-4}	5.183	0.475

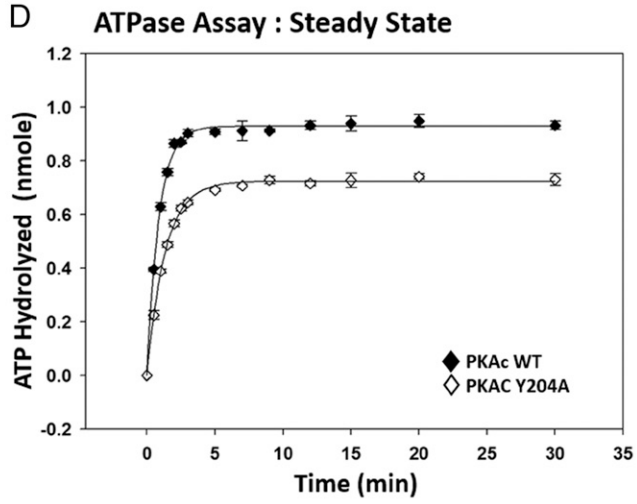

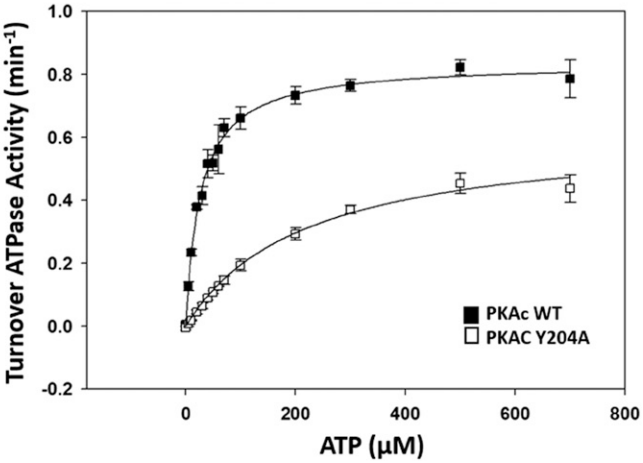

Fig. 2. Enzyme kinetic rates for the transfer of phosphate from ATP to substrate peptide or water for the Y204A vs. the wtPKA. (*A*) Kinetic plots for steady-state phosphotransfer assay for transfer of γ-PO_4 from ATP to Kemptide. (*B*) Kinetic plots for pre–steady-state phosphotransfer assay for transfer of γ-PO_4 from ATP to Kemptide. (*C*) Rate constants for the steady-state, pre–steady-state phosphotransfer assay, and steady ATPase assay. (*D*) Kinetic plots for steady-state ATPase assay for transfer of γ-PO_4 from ATP to water.

showed enhanced binding to all of the three nucleotides with lower K_D values (Fig. 3 and Fig. S3). As the affinity constants (K_D values) for AMP-PNP binding of Y204A (21.4 ± 1.5 μM) was comparable to the ATP binding of wtPKA (24.2 ± 2.2 μM), we studied the thermal stability of the two proteins upon ligand binding. This was done by differential scanning fluorimetry (DSF) using the Sypro-orange dye as an indicator (Fig. 4 and Fig. S4). For the apo proteins, it was estimated that the T_m for Y204A was ~5 °C less stable than the wtPKA (35.4 ± 0.2 °C for Y204A vs. 40.5 ± 0.2 °C for wtPKA). Upon AMP-PNP binding, the wtPKA was stabilized by 4 °C, whereas Y204A was comparably stabilized by 3 °C, indicating a similar mode of nucleotide binding. In another sample, the nucleotide-saturated proteins were incubated with the pseudosubstrate inhibitor peptide IP20 that is known to stabilize the wtPKA kinase. The wtPKA was stabilized by 6.1 °C compared with the apo protein, whereas the Y204A was stabilized by 4.7 °C.

Y204A Mutation Abolishes the Synergy Between Nucleotide and Peptide Binding at the Kinase Active Site. Biochemical studies using ATP indicated that the Y204A mutant was almost as efficient as the wtPKA in transferring the phosphate to water. The mutant was also able to bind the peptide as seen in the thermal melt experiments. It was hence pertinent to find the exact step where the mutant goes amiss in the catalytic cycle. To answer this question, we used the intrinsic property of PKA to use nucleotide and a pseudosubstrate peptide in a positively cooperative manner at the active site (20) (Fig. 5). We used a modified fluorescence polarization assay to measure PKA binding to a pseudosubstrate peptide (IP20) in tandem with the nucleotide (Fig. 5). This same pseudosubstrate peptide is present in the ternary complex of Y204A in its crystal. In the first assay, the protein (wtPKA and Y204A) was saturated with nucleotide and its binding to FAM-IP20 peptide was measured using the fluorescence from the FAM dye coupled to the peptide. In the corresponding flip assay, the proteins were first saturated with the FAM-IP20 and then binding of the nucleotide was measured against the background signal. In the case of the wtPKA, we could successfully recapitulate the positive cooperativity for nucleotide and peptide binding. wtPKA bound AMP-PNP with a K_D of 41.1 ± 3.0 μM (Fig. 3), but this affinity was enhanced by 1,000-fold in the presence of FAM-IP20 to a K_D of 66.5 ± 0.3 nM (Fig. 5). Strikingly, this synergy between the nucleotide and pseudosubstrate peptide binding was completely lost in the Y204A mutant. Y204A bound AMP-PNP in the presence of FAM-IP20 with a K_D of 44.7 ± 0.3 μM (Fig. 3), which is twofold worse than in the absence of FAM-IP20 (K_D of 21.4 ± 1.5 μM) (Fig. 5). The synergistic high-affinity binding of FAM-IP20 in the presence of saturating AMP-PNP was also lost in the Y204A mutant (K_D of 3.8 μM for Y204A vs. 1.9 nM for wtPKA). Also, in contrast to the Y204A crystal, the crystal of the ternary complex of wtPKA with ATP and IP20 has the γ-phosphate trapped in a very high-affinity complex at the active-site cleft in a fully closed conformation, presumably explaining why no hydrolysis of ATP was ever observed.

Simulations Show Altered Side-Chain Rotational Entropy for Y204A Active-Site Residues. The fluorescence polarization assay convincingly showed that Y204A mutant was able to bind the nucleotide and the pseudosubstrate inhibitor peptide individually but was unable to synergize the two at the active site. This meant that the entropic contributions from the internal dynamics of the protein could be flawed in maintaining the bisubstrate interaction. We hence analyzed the peptide dihedral angle and also the side-chain dihedral populations of crucial residues at the PKA active site. These included the conserved salt bridge of K72-E91, the DFG motif (D184), N171, D166, and the ATP binding K168 (Fig. 6). Y204A simulations show altered dihedral angles for the side chains of both K72 and E91, indicating an interference with the formation of a strong salt bridge compared with the wtPKA simulations. Similarly crucial rotamer differences can be seen for the active-site residues D184 and N171 (Fig. 6 and Figs. S5 and S6). Both of these residues must use specific rotamers to chelate the metal ions at the active site, using the first activating metal ion (Fig. 5) with the subsequent binding of second inhibitory metal ion (13). The binding of the second metal ion promotes its action as a Lewis base that must work on the β–γ bond of the ATP molecule to aid the removal of the terminal γ-PO_4 (31). Efficient binding of the two metal ions at the active site by residues N171 and D184

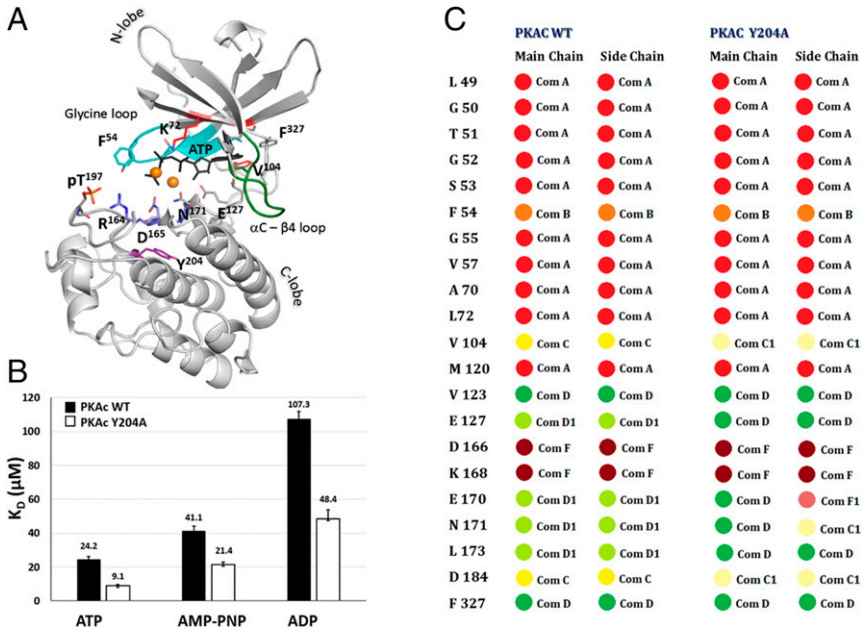

Fig. 3. Dynamics of nucleotide binding at the PKA active site. (*A*) ATP binding pocket of PKA. (*B*) Isothermal binding constants K_D for various nucleotides obtained for wtPKA and Y204. Isotherms are provided in Fig. S3. (*C*) Community structure for the main chains and side chains of residues lining the ATP binding pocket for wild-type PKA and Y204A mutant.

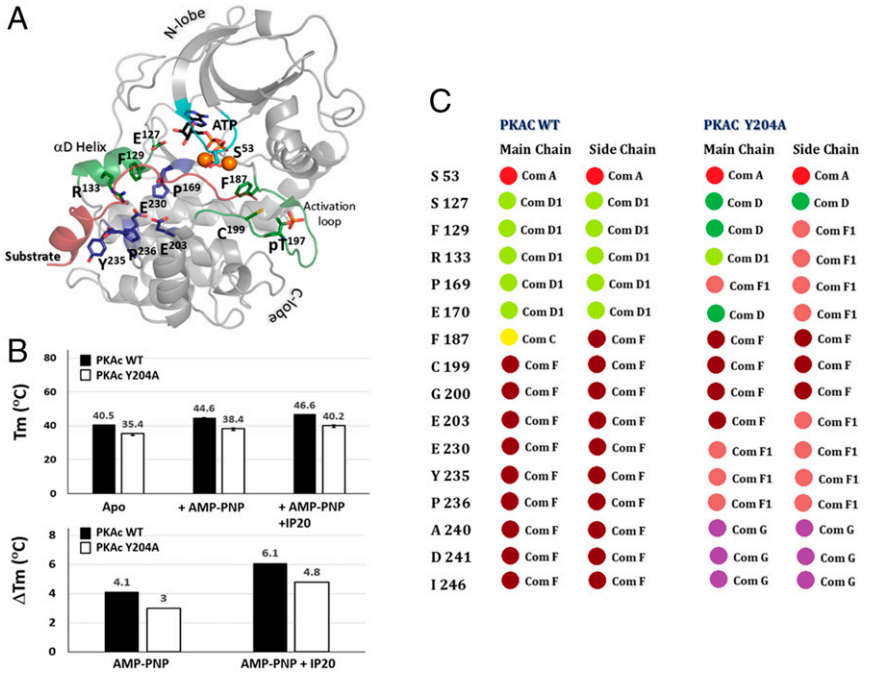

Fig. 4. Dynamics of pseudosubstrate binding at the PKA active-site cleft. (*A*) Pseudosubstrate peptide interacting residues at the PKA active-site cleft. (*B*) Stability of apo, binary (protein:nucleotide), and ternary (protein:nucleotide:pseudosubstrate) states of wtPKA and Y204A mutant as seen by differential scanning fluorimetry. Melt plots are provided in Fig. S4. (*C*) Community structure for the main chains and side chains of pseudosubstrate interacting residues for the wtPKA and Y204A mutant.

forms the basis of an efficient phosphotransfer process. However, for Y204A, these rotamers for D184 and N171 are not significantly populated as seen for the wtPKA. Consequently, the γ-phosphate of ATP is seen to occupy a presumably suboptimal conformation in the Y204A simulation compared with the wtPKA simulations (Movies S1 and S2). This rotational entropy and fluctuations in the residues at the active site of Y204A elaborate its altered internal conformational entropy that was unappreciated so far. In part, this was because the crystal structure of Y204A had the pseudosubstrate inhibitor IP20 bound to the structure that masked the dynamics of the γ-phosphate. These simulation analyses now also allow us to understand the extensively altered but previously unexplained H/D exchange seen throughout the Y204A molecule (Fig. 6 and Fig. S5).

Discussion

Eukaryotic protein kinases work as molecular switches that phosphorylate target proteins in response to a cellular signal. As in the case for most metabolic enzymes, the EPK bilobal structure was initially thought to stabilize the transition state at the active site, acting simplistically as a globular scaffold that supports the functioning of the kinase as a phosphotransferase. With the discovery of the hydrophobic spine architecture, the role of the bilobal structure has matured. Coupled with recent NMR analysis of the hydrophobic core, we now recognize that the core architecture creates an extended allosteric network that provides an effective mechanism to modulate kinase activity. Operating through a classic mechanical view, these allosteric changes have been attributed to changes in conformation of the structure that could be relayed to the active site through domino-type pathways (32). This view, however, fails to explain mutations, like the Y204A mutation explored here, that essentially do not reveal significant structural changes to protein conformation. The present study of Y204A has allowed us to revisit the allostery-based modulation of EPKs in a dynamics-based setting. As allostery is inherently thermodynamic, we emphasize here that it needs both structural (enthalpic) and dynamic (entropic) contributions, and measurements of structural parameters of the system alone do not account well for the role of protein conformational entropy (14). In the case of Y204A especially, the protein structure–function relationship is dominated by the protein internal motions that account for PKA's conformational entropy. Typically, studies on systems using enzyme substrate cycles have focused on unliganded or ligand-bound (initial or end-product) states. However, the key state that accounts for an enzyme's function is the intermediate ligand-bound state between the substrate and the products. In the present study, we have harnessed in silico approaches to create an intermediate ATP-1Mg^{2+}–bound structure of both wtPKA and Y204A for a comparison (Fig. 1). This forms the first step of the catalytic cycle when the kinase binds the nucleotide and first metal ion. Our previously presented work has suggested this closed ATP-1Mg^{2+}–bound form of PKA to be most allosterically coupled and having fewer communities compared with the open ATP-1Mg^{2+}–bound form or the ATP-2Mg^{2+}–bound form (22).

Our detailed steady-state and pre–steady-state enzyme catalysis experiments with Y204A have allowed for identification of the exact step of the PKA catalytic cycle that is fumbled by the Y204A mutant. Compared with wtPKA, the Y204A mutant binds nucleotides at its active site with an approximately twofold better affinity (Fig. 3) and can also transfer the γ-phosphate to water. This indicates the initial nucleotide-binding step in the PKA catalytic cycle, where the adenine ring completes the C spine, is unaltered in Y204A. This is supported by unaltered communities required for ATP binding (Com A and Com B) in Y204A dynamics. The community structure of the residues lining the ATP binding cleft, in particular the adenine binding pocket (Fig. 3), is also essentially unaltered with the exception of E170 and N171. However, it cannot be ruled out that the binding of nucleotide itself could be stabilizing the communities in Y204A as the maps are for the ATP-1Mg^{2+}–bound structure. A pre–steady-state phosphotransfer assay was performed to understand the burst phase for the catalytic cycle in Y204A (Figs. 2 and 5). This burst phase signifies stage III of the enzymes for its specific first single-turnover catalytic cycle (Fig. 5). In the wtPKA, this rate is significantly higher (285.3 ± 17.8 s^{-1})

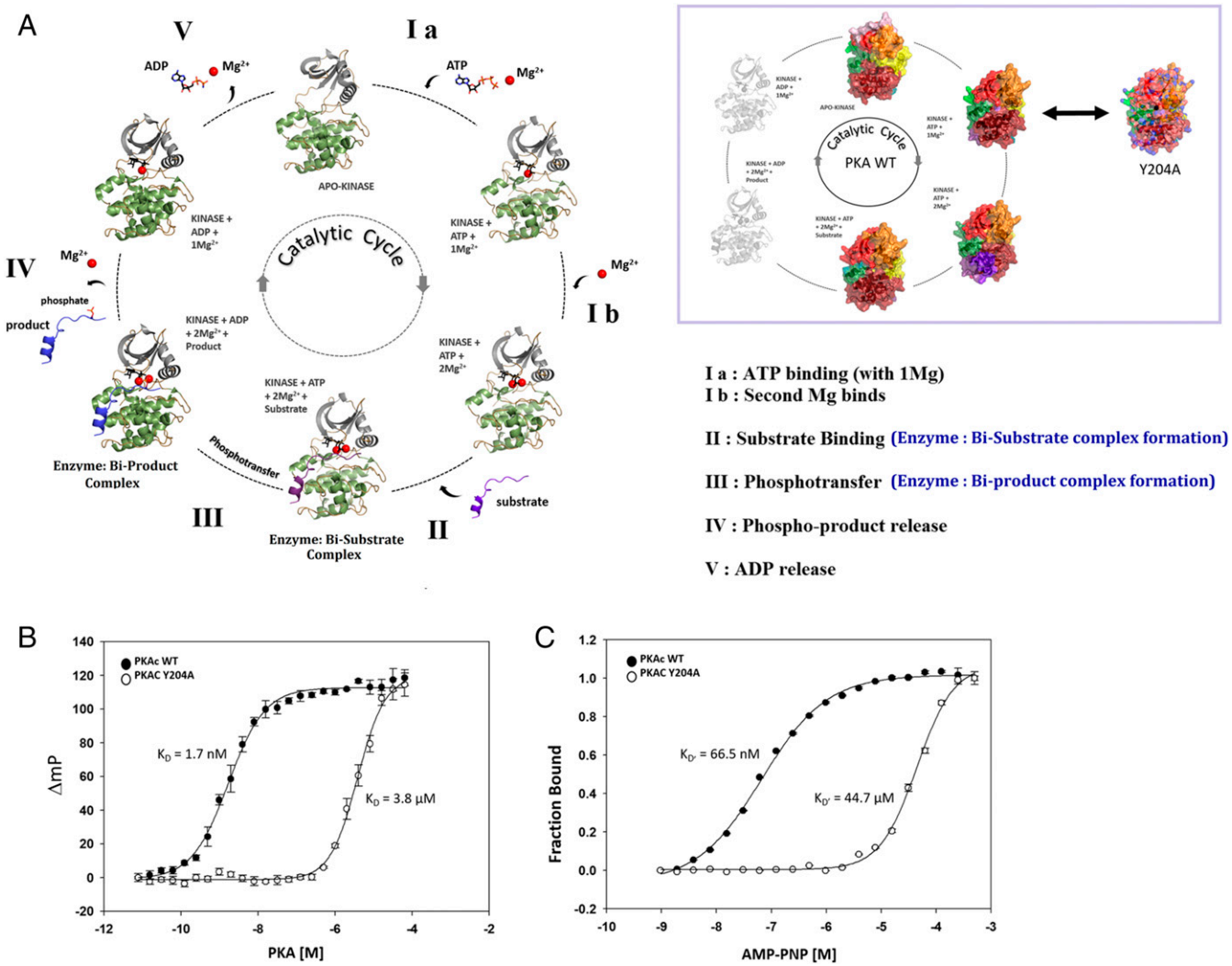

Fig. 5. Nucleotide and substrate synergy forms a pivotal aspect of the kinase reaction. (*A*) Kinase catalytic cycle described for PKA. Synergy between stages I and II form the basis of assay used in *B* and *C*. *Inset* shows the stage of the catalytic cycle used for community map analysis for comparing the dynamics of Y204A mutant with wtPKA. (*B*) Isotherm for binding of nucleotide saturated wild-type PKA vs. Y204A to FAM-IP20 by fluorescence polarization. (*C*) Isotherm for FAM-IP20 saturated wild-type PKA vs. Y204A to the nucleotide AMP-PNP as seen by fluorescence polarization.

than in the steady-state catalytic cycle (k_{cat} = 24.9 ± 0.2 s^{-1}) when the rate-limiting step becomes ADP release at stage V. Product release is also critically dependent on the second metal ion as the catalytic rate is much faster in the presence of low Mg^{2+} (33). Pre–steady-state kinetics for the Y204A mutant does not show a burst phase. Coupled to the results that Y204A binds ADP weaker than ATP at the active site, it is clear that the rate-limiting step for Y204A is no longer ADP release (Fig. 5, stage V).

We next tried to look for the properties of peptide binding for the Y204A protein. For this, we harnessed the positive cooperativity between nucleotide and peptide binding seen at the PKA active site (stage I and stage II of the catalytic cycle). For the wtPKA catalytic cycle, it is known that either nucleotide or peptide can bind to the kinase at stage I. This then enhances the affinity of the other molecule to bind the kinase at stage II, making a catalytic competent enzyme:bisubstrate complex (34). In our synergy assays using fluorescence polarization, we could recapitulate this scenario in solution for wtPKA and the pseudosubstrate inhibitor IP20 where we see a synergy of three orders of magnitude (Fig. 5). In the case of Y204A, however, the mutant could still bind the peptide (Fig. 4), but no further synergy was observed in the presence of nucleotide (Fig. 5). This narrowed down the rate-limiting step for Y204A to stages I and II of the catalytic cycle. As stage I was already established to be unaltered in the Y204A mutant as mentioned above, by elimination it was clear that the rate-limiting step for the Y204A mutant was stage II as opposed to stage V as seen for the wtPKA. Analysis of the peptide-binding communities for the ATP-$1Mg^{2+}$–bound wtPKA and Y204A dynamics demonstrated the differences that may affect the formation of a competent enzyme:bisubstrate complex at stage II of the catalytic cycle in Y204A (Fig. 4). First, the community for substrate/peptide binding (Com F) is split into two communities, ComF and ComF1, in Y204A. Crucial residues that may account for nucleotide and substrate synergy (S127, F129, R133, P169, F187) move from the catalytic community (Com D1) to become bridging residues between ComD and ComF1in Y204A. A closer inspection of the active-site residues (Fig. 6) shows that key residues (N171, D184, F187) essentially also switch communities altering the dynamic allostery of Y204A. Modified rotamer populations for active-site residues (K72, E91, N171, D166, D184, K168) provides an explanation for the transitioning of these residues from one community onto another.

The study presented here consolidates the enzyme catalytic reaction of PKA with its internal protein dynamics in a unique way,

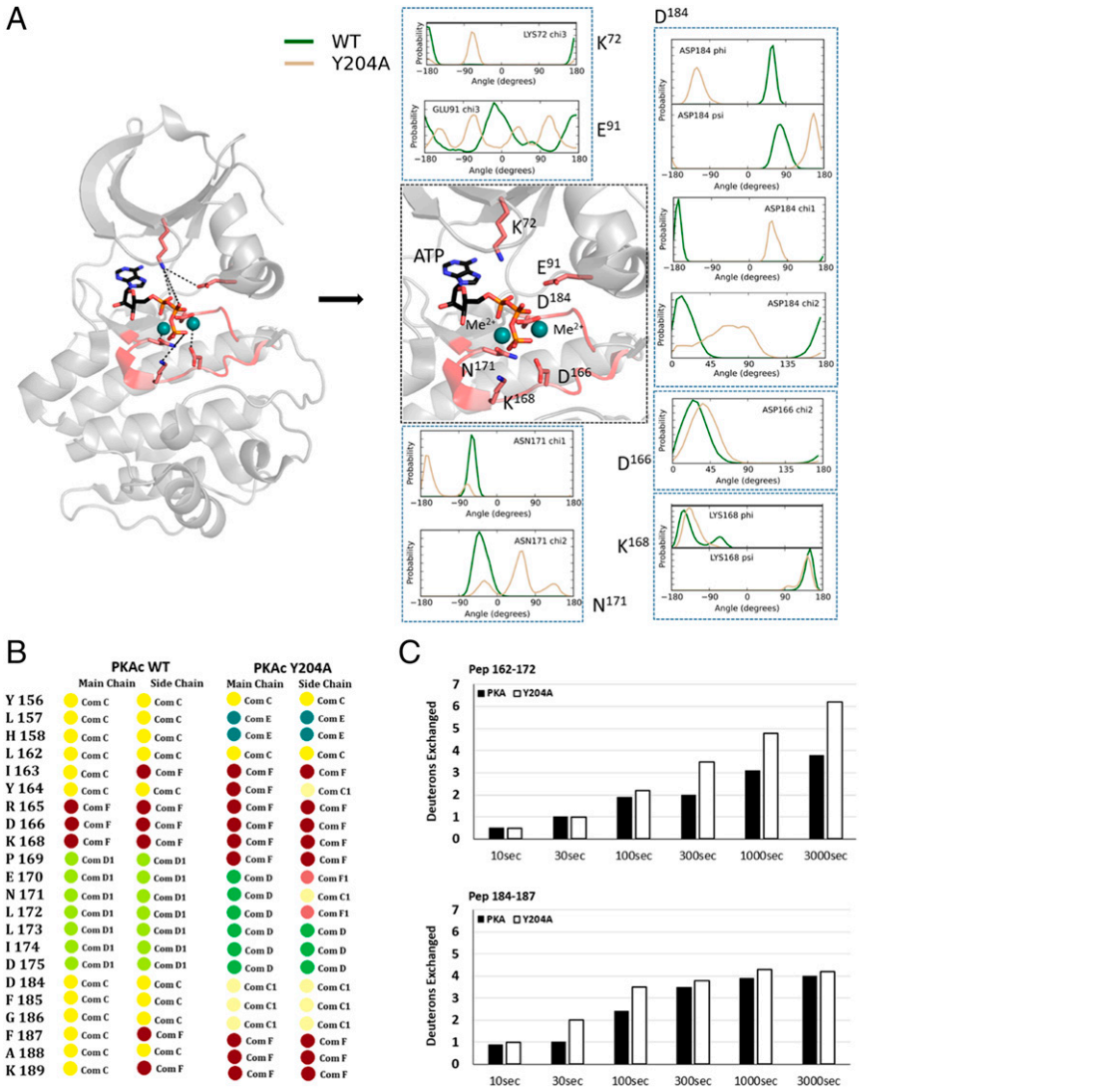

Fig. 6. Changes in conformational entropy of catalytic residues in Y204A. (*A*) Dihedral angles for main chains and side chains of catalytic residues that vary in their populations for the wild-type PKA simulations vs. Y204A mutant. Crucial catalytic residues have altered rotamer preferences in the Y204A dynamics as seen by their dihedral plots. (*B*) Community structure for the main chains and side chains of residues that line the active site cleft of connecting the two lobes of the kinase structure in wtPKA and Y204A. (*C*) H/D exchange seen for the active-site peptides 162–172 and 184–187 that show altered dynamics in molecular simulations (reproduced and adapted from ref. 19).

using a combination of traditional and modern tools. Our biochemical studies have helped identify the crucial node of depletion of activity in the Y204A catalytic cycle. Dynamic allostery-based community maps for this intermediate structure have then allowed us to appreciate the role of protein conformational entropy in the catalytic cycle. In summary, residues at the active site of the kinase are allosterically connected with the entire kinase molecule (Fig. 1), and all internal residue motions dictate catalytic activity. This study provides for a unique way for understanding mutations in EPKs that are identified in various diseases and cancers but are not well understood. We hope to extend this paradigm to these uncharacterized mutations of EPKs in our future work.

Materials and Methods

Mutagenesis and Protein Purification. Murine PKA catalytic subunit was cloned in the pET15b vector to obtain a recombinant PKA protein with an N-terminal poly-His tag. The Y204A mutation was created using the QuikChange II site-directed mutagenesis kit (Agilent Biotechnology). Both the wild-type and Y204A PKA constructs were transformed into *Escherichia coli* BL21(DE3) cells for efficient expression. The Y204A construct was cotransformed with GST-fused PDK1 kinase domain. This was done to ensure its proper folding upon phosphorylation at the activation loop Thr197 (35). Expression of PKA was confirmed by Western blot using monoclonal antibodies from BD Biosciences, whereas phosphorylation at the activation loop was confirmed by polyclonal anti-pThr197 antibodies from Invitrogen.

For large-scale protein purification, the transformed BL21(DE3) cells were grown in LB media at 37 °C to an OD of ~0.7 units at 600 nm. At this point, the cultures were induced with 0.25 mM isopropyl β-D-thiogalactopyranoside and incubated for 16 h at 16 °C overnight in a shaker incubator. Cultures were harvested and protein expression was confirmed by anti-PKA antibody from BD Biosciences. Cell pellet was suspended in lysis buffer containing 50 mM KH_2PO_4, 50 mM Tris·HCl, pH 8.0, 250 mM NaCl, 5% (vol/vol) glycerol, and 2 mM β-mercaptoethanol. Suspended cells were lysed under high pressure (18,000 psi) using a Microfluidizer (Microfluidics). The insoluble cell debris was separated from the soluble recombinant protein by centrifugation at 13,000 × *g* at 4 °C for 1 h in a fixed angle rotor. The supernatant was allowed to batch-bind with nickel-NTA bead (His-Select Resin; Sigma-Aldrich) in an end-to-end rotor for 3 h. The resin was washed with five bed volumes of lysis buffer followed by five bed volumes of wash buffer containing 50 mM imidazole. The protein was finally eluted in 50 mM KH_2PO_4, 50 mM Tris·HCl, 200 mM imidazole, pH 8.0, 250 mM NaCl, 5% glycerol, and 2 mM β-mercaptoethanol. Purity of the eluted fractions was checked by SDS/PAGE

gels. Eluted fractions were concentrated to 5 mL to be loaded onto a gel filtration column (Superdex 200; GE Healthcare). Buffer containing 50 mM Tris·HCl, pH 7.0, 250 mM NaCl, and 7% glycerol was used for the gel filtration. Purified protein was stable at 4 °C for about 10 days and at −20 °C for about a month when stored in 40% (vol/vol) glycerol.

Steady-State Phosphotransfer Assay. Steady-state phosphotransfer assay was done for the wtPKA and Y204A proteins in buffer containing 50 mM Mops, pH 6.8, 100 mM NaCl, 10 mM $MgCl_2$, and 2 mM DTT. For one set of the Michaelis–Menten conditions, ATP was kept constant at a concentration of 1 mM and Kemptide was varied from 0 to 250 μM. For the second set of Michaelis–Menten conditions, Kemptide was kept constant at a concentration of 1 mM and the nucleotide was varied from 0 to 250 μM. ^{32}P-ATP was used at a specific activity of 1,000 cpm/pmol and the enzyme concentration was used at 20 nM in a reaction volume of 15 μL. Phosphotransfer reaction was carried out for 3 min and quenched by addition of 85 μL of 30% acetic acid. One-half of the quenched reaction mixture (50 μL) was spotted on phosphocellulose disks and washed three times with 5% phosphoric acid. After a final wash with acetone, the filter disks were air dried and read on a liquid scintillation counter. Background radioactivity was measured by using a control with no ^{32}P-ATP. Data points obtained were fit to the Michaelis–Menten equation using the nonlinear regression module of SigmaPlot software (Systat Software).

Pre–Steady-State Phosphotransfer Assay. The pre–steady-state phosphotransfer kinetics was measured by KinTek RGF-3 quench flow apparatus as described previously (36). Briefly, the apparatus consist of three syringes connected to a stepping motor. The enzyme syringe consisted of protein concentration at 2 μM (2×) and Kemptide at 2 mM (2×). The ATP syringe contained ATP at 1 mM (2×) mixed with ^{32}P-ATP at specific activity of 500–1,000 cpm/pmol. The reaction buffer was 50 mM Mops, pH 6.8, 100 mM NaCl, 10 mM $MgCl_2$, and 2 mM DTT. Reactants are pushed into the reaction lines from these two distinct syringes, such that varying reaction lines and stepping motor speeds allow for capturing of extremely small reaction times (0.002–1 s). The third syringe carried the 30% acetic acid required to quench the kinase reaction. The quenched reaction mix was collected in a vial to be spotted onto a nitrocellulose disk. After washing these disks in phosphoric acid and acetone, the radioactive signal was measured by reading the filter disks on a liquid scintillation counter as described above. Background radioactivity was also read for each time point to be subtracted from the signal measured. The data obtained were fitted to the following equation using the nonlinear regression wizard of SigmaPlot software:

$$Y = \alpha[E]_t\{1 - \exp(-k_b t)\} + k_a t.$$

Here, Y is the product (phospho-Kemptide) formed, t is the time, $[E]_t$ is the total protein concentration, α is the "burst amplitude," k_b is the rate constant of the "burst phase," and k_a is the rate constant of the linear phase.

Nucleotide Binding Assay. Binding of wild-type and Y204A PKA kinase catalytic subunit to various nucleotides was ascertained by the changes in the kinase's intrinsic tryptophan fluorescence as described previously (37). The reaction buffer was used as 25 mM Mops, pH 7.0, 100 mM NaCl, 10 mM $MgCl_2$, and 2 mM DTT. ATP, ADP, and AMP-PNP stocks were directly made in the buffer and their concentration was confirmed by spectral measurements using an extinction coefficient of 15,400 $M^{-1}\cdot cm^{-1}$ at 260 nm. The 3.0 μM protein was incubated with increasing concentrations of nucleotide (0–250 μM) for 30 min, and the samples were read on a Jobin Yvon Horiba Fluorolog-3 spectrofluorometer. Samples were excited at the tryptophan excitation edge of 295 nm to minimize the inner filter effect. Emission spectra for the various samples were recorded from 300 to 400 nm. Decrease in the intrinsic tryptophan fluorescence on the protein upon nucleotide binding was fitted to a single ligand binding model of the nonlinear regression module from SigmaPlot software.

Steady-State ATP Hydrolysis Assay. ATP hydrolysis at the PKA active site (ATPase assay) was determined by the quantification of the inorganic phosphate released in the reaction. Reaction buffer was used as 25 mM Mops, pH 7.0, 100 mM NaCl, 10 mM $MgCl_2$, and 2 mM DTT. The 1.0 μM enzyme was incubated with increasing concentration of ATP (0–3.0 mM) to achieve Michaelis–Menten conditions. Reaction was stopped by the addition of Malachite Green reagent (Biomol Green; Enzo Lifesciences) after 15 min of incubation at room temperature (25 °C). For time course measurements, 1.0 μM enzyme was incubated with 500 μM ATP and the reaction was stopped at regular intervals using the Malachite Green reagent. Color was allowed to develop for another 15 min, and the reaction mixture was read at 650 nm using a UV-Vis spectrophotometer. A phosphate standard provided by the manufacturer of Biomol regent was used assess the nanomoles of inorganic phosphate present in the reaction mixtures. Steady-state Michaelis–Menten equations were used to calculate the K_m, k_{cat}, and $T_{1/2}$ of the ATPase reaction. All curves were fitted by using the nonlinear regression module of SigmaPlot Software.

Thermofluor Assay. Differential scanning fluorimetry (Thermofluor) assay was used to ascertain the stability and nucleotide and/or peptide binding of the wild type and Y204A mutant of PKA kinase. The reaction buffer was used as 25 mM Hepes, pH 7.0, 100 mM NaCl, 10 mM $MgCl_2$, and 1 mM DTT. Proteins were used at 2.0 μM, AMP-PNP was used at 1 mM, and pseudosubstrate peptide IP20 was used at 25 μM, as used previously for thermal melt experiments (38). Triplicate samples were prepared for apo protein, protein with nucleotide, and protein with nucleotide and peptide in a 96-well Q-PCR plate. Samples were chilled in ice for 10 min before addition of Sypro-orange dye (Invitrogen) at 5× concentration. Temperature scan mode of a CFX96 Touch Real-Time PCR Detection System (Bio-Rad) was used to heat the samples from 20 to 85 °C at a constant rate of 1 °C/min with a wait time of 1 min per 1 °C. Fluorescence from the bound Sypro-Orange dye was read using the FAM (492 nm) and ROX (610 nm) filters in real time (39). Sigmoidal melt curves were obtained according to the Boltzmann equation:

$$Y = L + (U - L)/(1 + \exp[(T_m - T)/\alpha]).$$

Here, Y is the fluorescence signal, T is the temperature, L and U are the upper and lower limits of fluorescent intensities, and α is the slope of the curve crossing the melting temperature, T_m. Curves were fitted to the sigmoidal nonregression equations of the SigmaPlot software to accurately determine the melting temperature (T_m).

Florescence Polarization Assay for Pseudosubstrate Inhibitor Peptide Binding. The wild type and Y204A mutant were tested for their pseudosubstrate binding ability using the fluorescence polarization assay. This protocol is inspired from a technique published earlier (40). FAM-labeled IP20 peptide was commercially purchased from Lifetein with ≥99% purity. Assay buffer was used as 25 mM Mops, pH 7.0, 35 mM NaCl, 5 mM $MgCl_2$, 1 mM DTT, and 0.02% Triton X-100. For the peptide binding assay, 5 nM of the FAM-IP20 peptide was titrated with varying concentrations of protein (7.3 pM to 64 μM) in the presence of 2 mM AMP-PNP. For the nucleotide cooperativity assay, 5 nM FAM-IP20 was incubated with 25 nM protein to be titrated with varying concentration of AMP-PNP (1 nm to 500 μM). All reactions were carried out in 150-μL volume in a black clear-bottom 96-well fluorescence plate. Samples were incubated for 2 h, and fluorescence readings were taken on a GeniosPro microplate reader (Tecan). Polarization was measured for the fluorescein dye [485-nm (20-nm bandwidth) excitation and 535-nm (20-nm bandwidth) emission filters] using the supplied dichroic mirror of the instrument. Fluorescence polarization was calculated in millipolarization units using the following equation:

$$P = 1{,}000 \times \{(I_{par} - G_f \times I_{per})/(I_{par} + G_f \times I_{per})\}.$$

Here, P is the polarization, I_{par} is the parallel intensity, and I_{per} is the intensity in the perpendicular direction. G factor (G_f) of the instrument was measured by using 1 nM fluorescein. Data obtained were plotted on a semilog scale and fitted to single ligand sigmoid curves of the nonlinear regression module of SigmaPlot software.

MD Simulations and Community Map Analysis. The high-resolution PKA kinase structure (Protein Data Bank ID code 3FJQ) was used for molecular dynamics simulations (22). The Y204 residue was mutated in silico to an alanine using a protein local optimization program and imported into Maestro (Schrodinger). Both structures were used in the protein:ATP:1Mg^{2+} complex form for the simulations. AMBER14 was used for energy minimization and equilibration using the pmemd.cuda module with hydrogen mass partitioning. Constant volume using mesh Ewald of 10 Å was used for the simulation. Temperature was increased from 0 to 300 K in linear time steps of 2.0 fs for over 5.0 ns and then maintained by the Langevin thermostat with a collision frequency of 1.0 ps^{-1}. Isotropic position scaling was used for constant pressure conditions. Position restraints were used for 100 ps (relaxation time, 360 ps), and then no position restraints were used for another 2.4 ns. Production simulations were run on a 512-node Anton supercomputer for 5.7 μs for wtPKA and 5.1 μs for the Y204A mutant. Cartesian mutual information for residues was used for the backbone carbons and an additional representative atom for each side chain to create a matrix using the MutInf software package. Kernel density estimation of the MutInf software (41) was used to calculate the dihedral

populations for all residues (main chain and side chain) for both the structures. The Girvan–Newman algorithm was used to identify the community structure for both the wtPKA and Y204A (21).

ACKNOWLEDGMENTS. We thank Prof. Joseph A. Adams for the use of the by KinTek RGF-3 quench flow equipment and Dr. Brandon Aubol for assistance with the same. This work was supported by Public Health Service/NIH Grant GM100310 (to G.V. and S.S.T.) and NIH Grant GM034921 (to S.S.T.). Anton computer time was provided by the National Center for Multiscale Modeling of Biological System through Grant P41GM103712-S1 from the NIH and the Pittsburgh Supercomputing Center (PSC). The Anton machine at PSC was generously made available by D. E. Shaw Research.

1. Manning G, Whyte DB, Martinez R, Hunter T, Sudarsanam S (2002) The protein kinase complement of the human genome. *Science* 298(5600):1912–1934.
2. Taylor SS, Kornev AP (2011) Protein kinases: Evolution of dynamic regulatory proteins. *Trends Biochem Sci* 36(2):65–77.
3. Adams JA (2001) Kinetic and catalytic mechanisms of protein kinases. *Chem Rev* 101(8):2271–2290.
4. Kornev AP, Taylor SS (2010) Defining the conserved internal architecture of a protein kinase. *Biochim Biophys Acta* 1804(3):440–444.
5. Kornev AP, Taylor SS, Ten Eyck LF (2008) A helix scaffold for the assembly of active protein kinases. *Proc Natl Acad Sci USA* 105(38):14377–14382.
6. Hu J, et al. (2015) Kinase regulation by hydrophobic spine assembly in cancer. *Mol Cell Biol* 35(1):264–276.
7. Adams JA (2003) Activation loop phosphorylation and catalysis in protein kinases: Is there functional evidence for the autoinhibitor model? *Biochemistry* 42(3):601–607.
8. Steichen JM, et al. (2012) Structural basis for the regulation of protein kinase A by activation loop phosphorylation. *J Biol Chem* 287(18):14672–14680.
9. Hyeon C, Jennings PA, Adams JA, Onuchic JN (2009) Ligand-induced global transitions in the catalytic domain of protein kinase A. *Proc Natl Acad Sci USA* 106(9):3023–3028.
10. Skora L, Mestan J, Fabbro D, Jahnke W, Grzesiek S (2013) NMR reveals the allosteric opening and closing of Abelson tyrosine kinase by ATP-site and myristoyl pocket inhibitors. *Proc Natl Acad Sci USA* 110(47):E4437–E4445.
11. Vajpai N, et al. (2008) Solution conformations and dynamics of ABL kinase-inhibitor complexes determined by NMR substantiate the different binding modes of imatinib/nilotinib and dasatinib. *J Biol Chem* 283(26):18292–18302.
12. Narayana N, Cox S, Nguyen-huu X, Ten Eyck LF, Taylor SS (1997) A binary complex of the catalytic subunit of cAMP-dependent protein kinase and adenosine further defines conformational flexibility. *Structure* 5(7):921–935.
13. Zheng J, et al. (1993) Crystal structure of the catalytic subunit of cAMP-dependent protein kinase complexed with MgATP and peptide inhibitor. *Biochemistry* 32(9):2154–2161.
14. Frederick KK, Marlow MS, Valentine KG, Wand AJ (2007) Conformational entropy in molecular recognition by proteins. *Nature* 448(7151):325–329.
15. Wand AJ (2013) The dark energy of proteins comes to light: Conformational entropy and its role in protein function revealed by NMR relaxation. *Curr Opin Struct Biol* 23(1):75–81.
16. Tzeng SR, Kalodimos CG (2012) Protein activity regulation by conformational entropy. *Nature* 488(7410):236–240.
17. Veglia G, Cembran A (2013) Role of conformational entropy in the activity and regulation of the catalytic subunit of protein kinase A. *FEBS J* 280(22):5608–5615.
18. Yang J, et al. (2005) Allosteric network of cAMP-dependent protein kinase revealed by mutation of Tyr204 in the P+1 loop. *J Mol Biol* 346(1):191–201.
19. Yang J, Ten Eyck LF, Xuong NH, Taylor SS (2004) Crystal structure of a cAMP-dependent protein kinase mutant at 1.26 Å: New insights into the catalytic mechanism. *J Mol Biol* 336(2):473–487.
20. Masterson LR, Mascioni A, Traaseth NJ, Taylor SS, Veglia G (2008) Allosteric cooperativity in protein kinase A. *Proc Natl Acad Sci USA* 105(2):506–511.
21. Srivastava AK, et al. (2014) Synchronous opening and closing motions are essential for cAMP-dependent protein kinase A signaling. *Structure* 22(12):1735–1743.
22. McClendon CL, Kornev AP, Gilson MK, Taylor SS (2014) Dynamic architecture of a protein kinase. *Proc Natl Acad Sci USA* 111(43):E4623–E4631.
23. Gasper PM, Fuglestad B, Komives EA, Markwick PR, McCammon JA (2012) Allosteric networks in thrombin distinguish procoagulant vs. anticoagulant activities. *Proc Natl Acad Sci USA* 109(52):21216–21222.
24. Chopra N, et al. (2016) Dynamic allostery mediated by a conserved tryptophan in the Tec family kinases. *PLoS Comput Biol* 12(3):e1004826.
25. Kornev AP, Taylor SS (2015) Dynamics-driven allostery in protein kinases. *Trends Biochem Sci* 40(11):628–647.
26. Knighton DR, et al. (1991) Crystal structure of the catalytic subunit of cyclic adenosine monophosphate-dependent protein kinase. *Science* 253(5018):407–414.
27. Knighton DR, et al. (1991) Structure of a peptide inhibitor bound to the catalytic subunit of cyclic adenosine monophosphate-dependent protein kinase. *Science* 253(5018):414–420.
28. Taylor SS, et al. (1988) cAMP-dependent protein kinase: Prototype for a family of enzymes. *FASEB J* 2(11):2677–2685.
29. Moore MJ, Adams JA, Taylor SS (2003) Structural basis for peptide binding in protein kinase A. Role of glutamic acid 203 and tyrosine 204 in the peptide-positioning loop. *J Biol Chem* 278(12):10613–10618.
30. Moore MJ, Kanter JR, Jones KC, Taylor SS (2002) Phosphorylation of the catalytic subunit of protein kinase A. Autophosphorylation versus phosphorylation by phosphoinositide-dependent kinase-1. *J Biol Chem* 277(49):47878–47884.
31. Valiev M, Yang J, Adams JA, Taylor SS, Weare JH (2007) Phosphorylation reaction in cAPK protein kinase-free energy quantum mechanical/molecular mechanics simulations. *J Phys Chem B* 111(47):13455–13464.
32. Yang J, et al. (2009) Contribution of non-catalytic core residues to activity and regulation in protein kinase A. *J Biol Chem* 284(10):6241–6248.
33. Herberg FW, Taylor SS (1993) Physiological inhibitors of the catalytic subunit of cAMP-dependent protein kinase: Effect of MgATP on protein-protein interactions. *Biochemistry* 32(50):14015–14022.
34. Li C, Ma N, Wang Y, Wang Y, Chen G (2014) Molecular dynamics simulation studies on the positive cooperativity of the Kemptide substrate with protein kinase A induced by the ATP ligand. *J Phys Chem B* 118(5):1273–1287.
35. Meharena HS, et al. (2013) Deciphering the structural basis of eukaryotic protein kinase regulation. *PLoS Biol* 11(10):e1001680.
36. Grant BD, Adams JA (1996) Pre-steady-state kinetic analysis of cAMP-dependent protein kinase using rapid quench flow techniques. *Biochemistry* 35(6):2022–2029.
37. Knape MJ, et al. (2015) Divalent metal ions Mg^{2+} and Ca^{2+} have distinct effects on protein kinase A activity and regulation. *ACS Chem Biol* 10(10):2303–2315.
38. Herberg FW, Doyle ML, Cox S, Taylor SS (1999) Dissection of the nucleotide and metal-phosphate binding sites in cAMP-dependent protein kinase. *Biochemistry* 38(19):6352–6360.
39. Niesen FH, Berglund H, Vedadi M (2007) The use of differential scanning fluorimetry to detect ligand interactions that promote protein stability. *Nat Protoc* 2(9):2212–2221.
40. Saldanha SA, Kaler G, Cottam HB, Abagyan R, Taylor SS (2006) Assay principle for modulators of protein-protein interactions and its application to non-ATP-competitive ligands targeting protein kinase A. *Anal Chem* 78(24):8265–8272.
41. McClendon CL, Hua L, Barreiro A, Jacobson MP (2012) Comparing conformational ensembles using the Kullback-Leibler divergence expansion. *J Chem Theory Comput* 8(6):2115–2126.